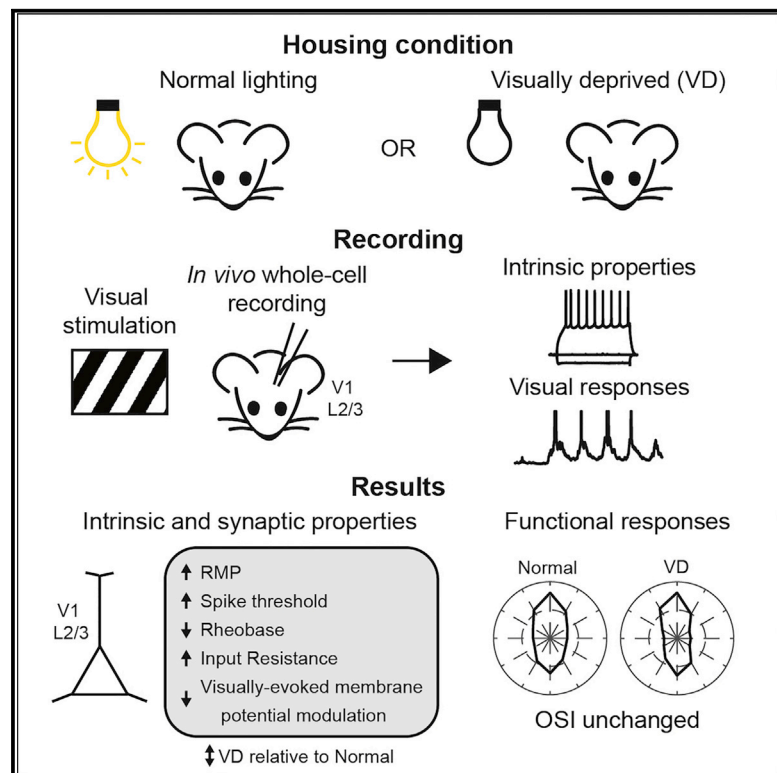


Visual Experience Regulates the Intrinsic Excitability of Visual Cortical Neurons to Maintain Sensory Function

Graphical Abstract



Authors

Alexander P.Y. Brown, Lee Cossell,
Troy W. Margrie

Correspondence

t.margrie@ucl.ac.uk

In Brief

This large-scale *in vivo* study by Brown et al. shows that the intrinsic and synaptic properties of V1 layer 2/3 neurons are modulated by ongoing visual input. However, despite significant changes in cellular intrinsic and synaptic properties after visual deprivation, overall functional selectivity for oriented stimuli remains unchanged.

Highlights

- Intrinsic properties of V1 L2/3 neurons are modulated by ongoing sensory input
- Visually evoked synaptic responses are reduced after visual deprivation
- Deprivation has little effect on spiking or subthreshold orientation selectivity
- Cortical cells preserve sensory function despite long-term changes in synaptic drive



Visual Experience Regulates the Intrinsic Excitability of Visual Cortical Neurons to Maintain Sensory Function

Alexander P.Y. Brown,^{1,2} Lee Cossell,^{1,2} and Troy W. Margrie^{1,3,*}

¹The Sainsbury Wellcome Centre for Neural Circuits and Behaviour, University College London, 25 Howland Street, London W1T 4JG, UK

²These authors contributed equally

³Lead Contact

*Correspondence: t.margrie@ucl.ac.uk

<https://doi.org/10.1016/j.celrep.2019.03.073>

SUMMARY

This *in vivo* study shows that both intrinsic and sensory-evoked synaptic properties of layer 2/3 neurons in mouse visual cortex are modified by ongoing visual input. Following visual deprivation, intrinsic properties are significantly altered, although orientation selectivity across the population remains unchanged. We, therefore, suggest that cortical cells adjust their intrinsic excitability in an activity-dependent manner to compensate for changes in synaptic drive and maintain sensory network function.

INTRODUCTION

Local network activity can influence the biophysical properties of constituent neurons (Angelo et al., 2012), and the homeostatic mechanisms that serve to maintain cellular excitability are crucial to ensuring stable network function (Marder and Goaillard, 2006). Recordings from neurons *in vitro* show that the biophysical profile of a given cell can be influenced by recent activity (Desai et al., 1999; Marder and Goaillard, 2006; Maffei and Turrigiano, 2008; Nataraj et al., 2010) and that such intrinsic plasticity can alter the response to input (Desai et al., 1999; Turrigiano et al., 1994; Sjöström et al., 2008). In the mammalian brain, although experience-dependent changes in cellular excitability are partly dependent on changes at synapses (Desai et al., 2002; Goel and Lee, 2007; Hofer et al., 2009), no study has yet investigated whether externally driven activity might drive intrinsic changes *in vivo* or how this could be used to optimize or maintain physiological function, for example a particular output, such as overall firing rate (Turrigiano and Nelson, 2004; Keck et al., 2013; Kuhlman et al., 2013; Hengen et al., 2013; Barnes et al., 2015; Gainey and Feldman, 2017).

RESULTS

To explore this question, we performed whole-cell recordings from layer 2/3 regular-spiking neurons in primary visual cortex of anaesthetized mice that, post-weaning, had either been housed under normal lighting conditions (control, 12 h light/12 h dark; n = 150 cells from 110 mice) or in complete darkness

for up to five weeks (visually deprived [V.D.]; n = 40 cells from 13 mice). We observed that V.D. mice had significantly depolarized resting membrane potentials (median control: -76.8 mV (interquartile range, IQR: 9.0 mV) versus V.D.: -71.6 mV (IQR: 9.6 mV); $p = 0.0019$ Wilcoxon rank-sum test; Figures 1A and 1B) and spike threshold (control: -27.9 mV (IQR: 10.4 mV) versus V.D.: -24.3 mV (IQR: 9.7 mV); $p = 1.4 \times 10^{-4}$; Figures 1A and 2C) compared to control mice. Although the resting membrane potential and spike threshold both shifted to more depolarized potentials in the absence of visual input, the distance from rest to threshold did not change (control: 49.1 mV (IQR: 11.7 mV) versus V.D.: 48.9 mV (IQR: 15.4 mV); $p = 0.64$; Figure 1D). Furthermore, neurons in V.D. animals exhibited an increased input resistance to depolarizing (control: 87.0 M Ω (IQR: 51.3 M Ω), n = 128 versus V.D.: 104.7 M Ω (IQR: 68.1 M Ω), n = 35; $p = 0.019$; Figures 1E and 1F) but not hyperpolarizing current injections (control: 51.4 M Ω (IQR: 30.8 M Ω), n = 150 versus V.D.: 52.9 M Ω (IQR: 36.6 M Ω), n = 40; $p = 0.71$) and, subsequently, showed lower rheobase values (control: 275 pA (IQR: 125 pA) versus V.D.: 225 pA (IQR: 87.5 pA); $p = 0.0086$; Figure 1G) suggesting that active conductances responsible for rectification in L2/3 cells are altered following changes in visual input. There was no correlation between the duration of visual deprivation (range: 18–34 days) and any of the intrinsic properties tested (resting membrane potential: Spearman's $\rho = -0.08$, $p = 0.63$; spike threshold: $\rho = 0.11$, $p = 0.52$; distance from resting potential to spike threshold: $\rho = 0.09$, $p = 0.57$; rheobase: $\rho = 0.11$, $p = 0.50$; or hyperpolarizing input resistance: $\rho = -0.26$, $p = 0.11$; all n = 40).

To understand how such cellular changes might impact function, in a subset of cells we also quantified the visually evoked synaptic and spiking responses to moving grating stimuli (control: n = 128 neurons from 98 mice; V.D.: n = 35 neurons from 13 mice) (Figure 2A). For each grating direction, we quantified the average evoked synaptic depolarization (V_{m0} ; Figures 2A and 2B), the modulation of the synaptic response (V_{m1} ; Figures 2A and 2C) and the mean spike rate (Figure 2D). Although there was little change in the overall amount of depolarization (V_{m0} at preferred spiking direction: control 11.2 mV (IQR: 6.8 mV) versus V.D. 10.1 mV (IQR: 3.6 mV), $p = 0.10$; Wilcoxon rank-sum test; Figure 2B), there was a significant decrease in the amount of membrane potential modulation (V_{m1} at preferred, control 11.0 mV (IQR: 7.9 mV) versus V.D. 7.2 mV (IQR: 5.8 mV), $p = 9.1 \times 10^{-4}$; Figure 2C). Cells recorded from animals



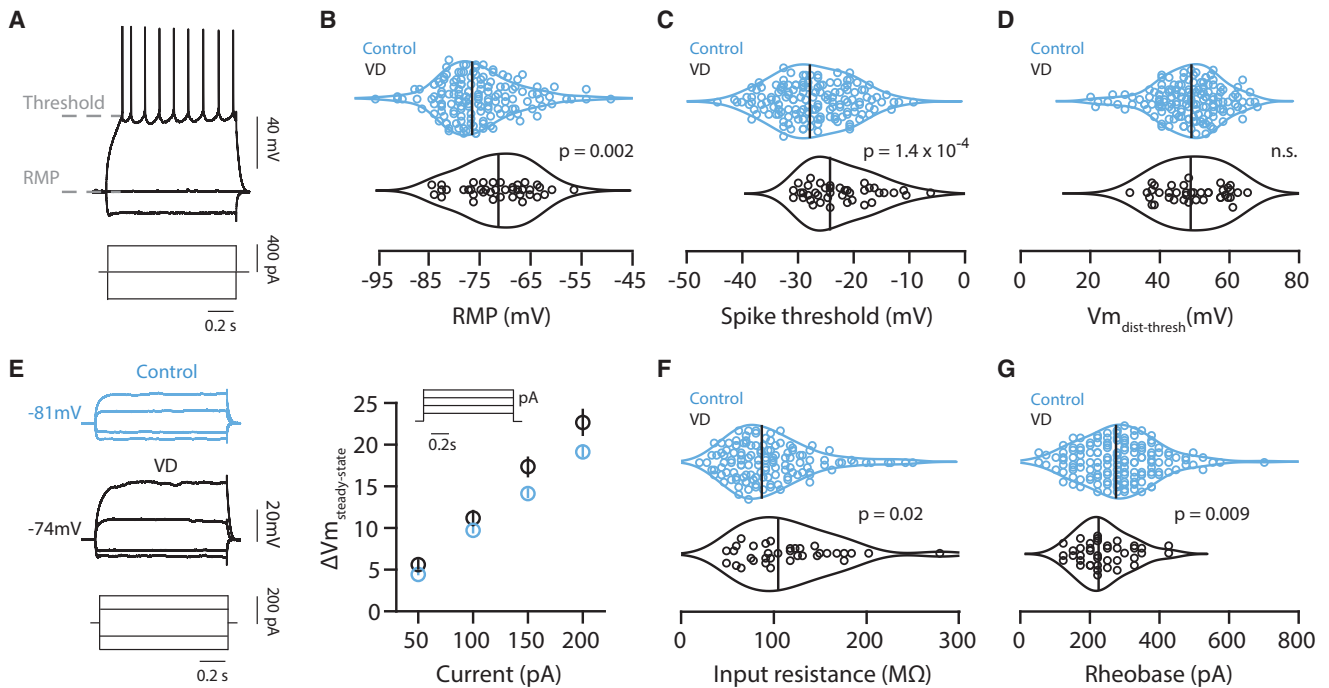


Figure 1. Intrinsic Membrane Properties of Layer 2/3 Pyramidal Cells Are Altered in Visually Deprived Mice

(A) Example membrane potential traces evoked by hyperpolarizing and depolarizing current steps. (B–D) Violin plots of resting membrane potential (B), spike threshold at rheobase (C), and distance between resting membrane potential and spike threshold (D) recorded in control (blue) and visually deprived (black) mice. (E) Left, example membrane potential traces in response to hyperpolarizing and depolarizing current steps recorded in control and visually deprived mice. Right, graph showing the amplitude of the steady-state membrane potential evoked by depolarizing current steps. (F and G) Violin plots of input resistance (F) and rheobase (G). Vertical bars on the violin plots indicate median values. (E, right) Data are mean \pm SEM. Where significant, p values from the Wilcoxon rank-sum test are shown. Scale bars in (A) and (E) are labelled.

with reduced visual input also show a reduction in evoked spike rates (spike rate at preferred, control 2.15 Hz (IQR: 4.86 Hz) versus V.D. 0.95 Hz (IQR: 2.34 Hz); $p = 0.0058$; Figure 2D), and the number of neurons without visually evoked spikes significantly increased compared to control (control: 1/128 versus V.D: 7/35; $p < 0.0001$, Fisher's exact test). Thus, reducing visual input alters not only intrinsic set points such as resting membrane potential and threshold but also modifies both the synaptic and spiking responsiveness of cells. It is not possible to discern from these data whether the reduced input modulation is due to a decrease in driving force caused by more depolarized potentials or synaptic strength. In any case, increased input resistance is expected to at least partly counteract these effects.

Although there were significant decreases in membrane potential modulation and firing rate, cells recorded from V.D. animals showed tuning responses that appeared very similar to those recorded in control animals (Figure 2E). To examine this in detail, we quantified the degree of orientation tuning of V_{m0} ($OSI_{V_{m0}}$; Figure 2F), V_{m1} ($OSI_{V_{m1}}$; Figure 2G), and the resultant spiking (OSI_{F0} ; Figure 2H). Despite having been housed in complete darkness for up to five weeks, we found that the distribution of OSIs was similar between control and V.D. mice for all OSI measures ($OSI_{V_{m0}}$, $p = 0.26$ (all neurons included); $OSI_{V_{m1}}$, $p = 0.95$ (all neurons included); OSI_{F0} $p = 0.96$ (control:

$n = 111$, V.D.: $n = 25$; see STAR Methods), Kolmogorov-Smirnov tests; Figures 2F–2H). Thus, although intrinsic and visually evoked synaptic and spiking responses are altered, selectivity for moving gratings of different orientations remained unaffected by visual deprivation.

We next sought to identify what specific cellular parameters might contribute to this preservation of function in the absence of ongoing visual input by performing a series of correlation analyses between cellular properties and orientation tuning across the control and deprived populations. In control mice, the resting membrane potential (Spearman's $\rho = -0.51$, $n = 111$, $p = 1.1 \times 10^{-8}$), threshold ($\rho = -0.29$, $n = 111$, $p = 0.0018$) and the distance from rest to spiking threshold ($\rho = 0.47$, $n = 111$, $p = 1.8 \times 10^{-7}$) were strongly correlated with OSI_{F0} (Figure 3A; Figures S1A and S1B). Unexpectedly, the resting membrane potential and its distance to threshold were found to be more strongly correlated with spiking orientation tuning than the orientation tuning, as measured from the underlying synaptic responses ($OSI_{V_{m0}}$ versus OSI_{F0} : $\rho = 0.35$, $n = 111$ $p = 1.5 \times 10^{-4}$, $OSI_{V_{m1}}$ versus OSI_{F0} : $\rho = 0.43$, $n = 111$, $p = 2.6 \times 10^{-6}$; Figure 3A). Overall, most relationships between intrinsic and synaptic parameters were similar in control and V.D. animals (Figure 3A). However, the relationship between the distance from rest to threshold and OSI_{F0}

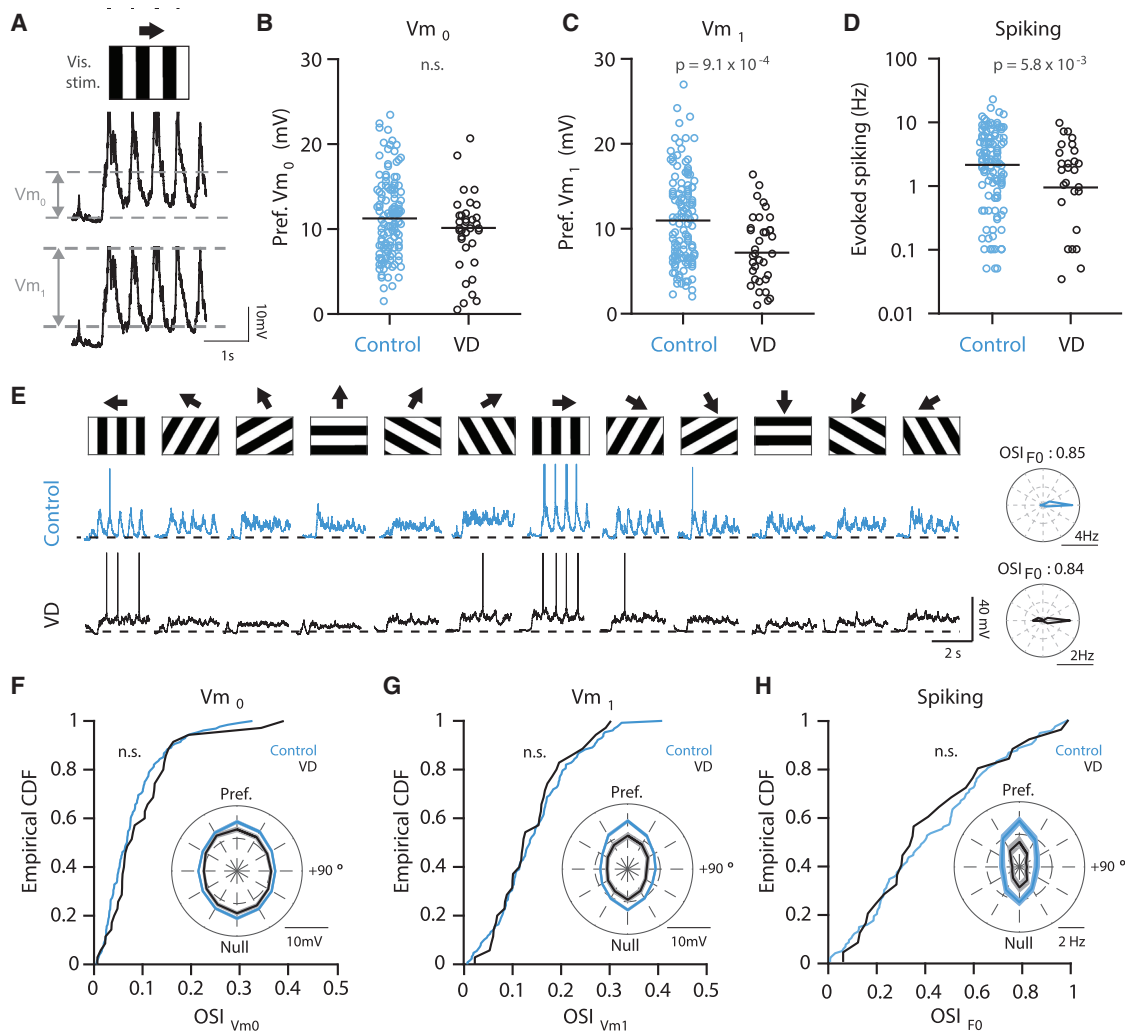


Figure 2. Reduced Synaptic and Spiking Responses but No Change in Selectivity in Visually Deprived Mice

(A) Example (spike-clipped) membrane potential trace recorded in response to a drifting grating stimulus, showing the evoked mean membrane potential depolarization (V_{m0}) and modulation (V_{m1}).

(B–D) Plots showing the V_{m0} (B), the V_{m1} (C), and spike rate in all cells that showed evoked spikes (D) measured at the preferred direction for spiking in control (blue) and visually deprived (black) mice. (D) Plotted on a logarithmic scale. (B–D) Horizontal line indicates median.

(E) Membrane potential traces evoked by drifting gratings (moving in twelve different directions; top) for two example cells recorded in either control (blue) or deprived mice (black).

(F–H) Cumulative histograms showing the distributions of OSI values for V_{m0} (F), V_{m1} (G), and spiking (H). Inset, polar plots showing the average tuning profile (aligned to the preferred direction for spiking) for all cells recorded in control (blue) or visually deprived (black) mice. (F–H, insets) Data are displayed as the mean \pm SEM.

Where significant, p values from the Wilcoxon rank-sum test (B–D) and Kolmogorov-Smirnov test (F–H) are shown. Scale bars in (A) and (E)–(H) are labelled.

decreased significantly in the absence of visual input (V.D.: $\rho = -0.03$, $p = 0.90$, $n = 25$; versus control Fisher's $Z = 2.30$, $p = 0.021$; Figure 3A; Figure S1A). On the other hand, in V.D. animals resting membrane potential maintained its strong correlation, while V_{m1} became significantly more correlated with OSI_{F0} (control: $\rho = 0.30$, $n = 111$, $p = 0.0013$; versus V.D.: $\rho = 0.67$, $n = 25$, $p = 3.2 \times 10^{-4}$; Fisher's $Z = 2.16$, $p = 0.031$) (Figure 3A; Figure S1C). This suggests that a cell's resting membrane potential and membrane potential modulation are key parameters in retaining the functional profile of visual neurons (Figure 3B).

DISCUSSION

By performing whole-cell recordings from large numbers of layer 2/3 cells in primary visual cortex, we have identified several cellular properties that are regulated by ongoing sensory input *in vivo*. This large dataset has revealed strong correlations between sensory function and several intrinsic properties. Notably, there was a strong correlation between the selectivity for orientated stimuli and both the distance of the resting membrane potential from spike threshold and the resting membrane potential itself. Indeed, under control conditions, we observed

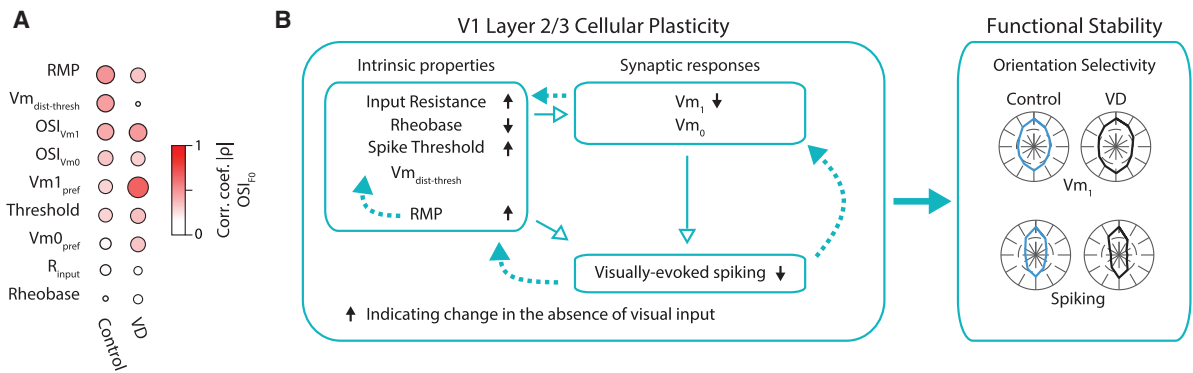


Figure 3. Proposed Cellular Mechanisms Underlying the Maintenance of Orientation Selectivity

(A) Plots showing the relationship between intrinsic and synaptic properties and spiking OSI in normal (left column) and visually deprived (middle column) mice. Color and size of circle indicate the Spearman's correlation coefficient (absolute value). Variables are ranked by correlation (p value) in the control group.

(B) Schematic describing the changes in intrinsic and synaptic properties in layer 2/3 neurons resulting from reduced visual input. Visual-input-dependent homeostatic plasticity of these intrinsic properties (dashed arrows) is proposed to maintain robust orientation selectivity. Polar plots display an average tuning (scaled to the peak response at the preferred direction in control) obtained from all cells recorded in this study. See also Figure S1.

correlations between intrinsic and functional properties that have not been previously identified (Wilson et al., 2016) likely because of insufficient statistical power. Furthermore, when comparing the functional responses and intrinsic properties of dark-reared animals, we find that the substantial changes in input resistance and subsequent decrease in rheobase appear to compensate for reduced network excitability while functional stability across the population persists (Marder and Goaillard, 2006).

Rather than investigating loss of input effects in animals that have been dark reared from before eye opening, the deprivation protocol used here was designed to perturb the system rather than ensure animals were completely naive to visual input. Studies that have examined brief periods of visual deprivation have shown that periods of darkness can reverse molecular signatures of maturation in the visual cortex, such as NMDA receptor composition (He et al., 2006), the expression of brain-derived neurotrophic factor (Castrén et al., 1992), as well as elements of the cytoskeleton (Duffy and Mitchell, 2013) and inhibitory network (Erchova et al., 2017). Such changes may return the cortex to an immature state, reinstating critical periods (Cynader and Mitchell, 1980; Mower, 1991) and enabling greater plasticity (He et al., 2007; Medini, 2014). Furthermore, neurons recorded from slices of immature rat L5 visual cortex have more depolarized resting membrane potentials and higher input resistances than in mature rat (Etherington and Williams, 2011), consistent with our findings and the fact that the cortex adopts a more juvenile-like state after periods of visual deprivation.

The cell's resting membrane potential was identified as one key parameter that might trigger such plasticity. Various membrane-potential-related sources of intracellular Ca²⁺ could drive such changes. These include spiking and backpropagating action potentials (Stuart and Spruston, 2015) and subthreshold sources, such as NMDA channels (Smith et al., 2013) and low-voltage-dependent Ca²⁺ channels (Nanou and Catterall, 2018). Regardless of the precise mechanisms, the fact that synaptic tuning is maintained suggests such intrinsic plasticity has a global impact to preserve the relative weights of visually evoked synaptic inputs across the dendritic tree. We propose that, under

conditions of reduced sensory input, changes in intrinsic properties, including resting membrane potential, trigger cellular plasticity (Mahon et al., 2003; Mahon and Charpier, 2012) to ensure that functional properties, such as orientation tuning, are retained.

STAR★METHODS

Detailed methods are provided in the online version of this paper and include the following:

- KEY RESOURCES TABLE
- CONTACT FOR REAGENT AND RESOURCE SHARING
- EXPERIMENTAL MODEL AND SUBJECT DETAILS
- METHOD DETAILS
 - Surgical procedures
 - *In vivo* whole-cell recordings
 - Response to current injection
 - Visual stimulation
 - Visual deprivation
 - Data Analysis
- QUANTIFICATION AND STATISTICAL ANALYSIS
- DATA AND SOFTWARE AVAILABILITY

SUPPLEMENTAL INFORMATION

Supplemental Information can be found online at <https://doi.org/10.1016/j.celrep.2019.03.073>.

ACKNOWLEDGMENTS

We are grateful to the support staff of the Biological Research Facility and thank Tiago Branco and Mateo Vélez-Fort for providing comments on the manuscript. This work was funded by an Investigator Award from the Wellcome Trust (096436/B/11/Z) (T.W.M.).

AUTHOR CONTRIBUTIONS

T.W.M. and A.P.Y.B. designed and A.P.Y.B. performed experiments. A.P.Y.B. and L.C. analyzed the data. L.C., A.P.Y.B., and T.W.M. wrote the manuscript.

DECLARATION OF INTERESTS

The authors declare no competing interests.

Received: November 30, 2018

Revised: February 18, 2019

Accepted: March 20, 2019

Published: April 16, 2019

REFERENCES

- Angelo, K., Rancz, E.A., Pimentel, D., Hundahl, C., Hannibal, J., Fleischmann, A., Pichler, B., and Margrie, T.W. (2012). A biophysical signature of network affiliation and sensory processing in mitral cells. *Nature* 488, 375–378.
- Barnes, S.J., Sammons, R.P., Jacobsen, R.I., Mackie, J., Keller, G.B., and Keck, T. (2015). Subnetwork-specific homeostatic plasticity in mouse visual cortex in vivo. *Neuron* 86, 1290–1303.
- Castrén, E., Zafra, F., Thoenen, H., and Lindholm, D. (1992). Light regulates expression of brain-derived neurotrophic factor mRNA in rat visual cortex. *Proc. Natl. Acad. Sci. USA* 89, 9444–9448.
- Cynader, M., and Mitchell, D.E. (1980). Prolonged sensitivity to monocular deprivation in dark-reared cats. *J. Neurophysiol.* 43, 1026–1040.
- Desai, N.S., Rutherford, L.C., and Turrigiano, G.G. (1999). Plasticity in the intrinsic excitability of cortical pyramidal neurons. *Nat. Neurosci.* 2, 515–520.
- Desai, N.S., Cudmore, R.H., Nelson, S.B., and Turrigiano, G.G. (2002). Critical periods for experience-dependent synaptic scaling in visual cortex. *Nat. Neurosci.* 5, 783–789.
- Duffy, K.R., and Mitchell, D.E. (2013). Darkness alters maturation of visual cortex and promotes fast recovery from monocular deprivation. *Curr. Biol.* 23, 382–386.
- Erchova, I., Vasalaukaite, A., Longo, V., and Sengpiel, F. (2017). Enhancement of visual cortex plasticity by dark exposure. *Philos. Trans. R. Soc. Lond. B Biol. Sci.* 372, 20160159.
- Etherington, S.J., and Williams, S.R. (2011). Postnatal development of intrinsic and synaptic properties transforms signaling in the layer 5 excitatory neural network of the visual cortex. *J. Neurosci.* 31, 9526–9537.
- Gainey, M.A., and Feldman, D.E. (2017). Multiple shared mechanisms for homeostatic plasticity in rodent somatosensory and visual cortex. *Philos. Trans. R. Soc. Lond. B Biol. Sci.* 372, 20160157.
- Goel, A., and Lee, H.K. (2007). Persistence of experience-induced homeostatic synaptic plasticity through adulthood in superficial layers of mouse visual cortex. *J. Neurosci.* 27, 6692–6700.
- He, H.-Y., Hodos, W., and Quinlan, E.M. (2006). Visual deprivation reactivates rapid ocular dominance plasticity in adult visual cortex. *J. Neurosci.* 26, 2951–2955.
- He, H.-Y., Ray, B., Dennis, K., and Quinlan, E.M. (2007). Experience-dependent recovery of vision following chronic deprivation amblyopia. *Nat. Neurosci.* 10, 1134–1136.
- Hengen, K.B., Lambo, M.E., Van Hooser, S.D., Katz, D.B., and Turrigiano, G.G. (2013). Firing rate homeostasis in visual cortex of freely behaving rodents. *Neuron* 80, 335–342.
- Hofer, S.B., Mrsic-Flogel, T.D., Bonhoeffer, T., and Hübener, M. (2009). Experience leaves a lasting structural trace in cortical circuits. *Nature* 457, 313–317.
- Keck, T., Keller, G.B., Jacobsen, R.I., Eysel, U.T., Bonhoeffer, T., and Hübener, M. (2013). Synaptic scaling and homeostatic plasticity in the mouse visual cortex in vivo. *Neuron* 80, 327–334.
- Kuhlman, S.J., Olivas, N.D., Tring, E., Ikrar, T., Xu, X., and Trachtenberg, J.T. (2013). A disinhibitory microcircuit initiates critical-period plasticity in the visual cortex. *Nature* 501, 543–546.
- Levelt, C.N., and Hübener, M. (2012). Critical-period plasticity in the visual cortex. *Annu. Rev. Neurosci.* 35, 309–330.
- Maffei, A., and Turrigiano, G.G. (2008). Multiple modes of network homeostasis in visual cortical layer 2/3. *J. Neurosci.* 28, 4377–4384.
- Mahon, S., and Charpier, S. (2012). Bidirectional plasticity of intrinsic excitability controls sensory inputs efficiency in layer 5 barrel cortex neurons in vivo. *J. Neurosci.* 32, 11377–11389.
- Mahon, S., Casassus, G., Mulle, C., and Charpier, S. (2003). Spike-dependent intrinsic plasticity increases firing probability in rat striatal neurons in vivo. *J. Physiol.* 550, 947–959.
- Marder, E., and Goaillard, J.M. (2006). Variability, compensation and homeostasis in neuron and network function. *Nat. Rev. Neurosci.* 7, 563–574.
- Margrie, T.W., Brecht, M., and Sakmann, B. (2002). In vivo, low-resistance, whole-cell recordings from neurons in the anaesthetized and awake mammalian brain. *Pflugers Arch.* 444, 491–498.
- Medini, P. (2014). Experience-dependent plasticity of visual cortical microcircuits. *Neuroscience* 278, 367–384.
- Mower, G.D. (1991). The effect of dark rearing on the time course of the critical period in cat visual cortex. *Brain Res. Dev. Brain Res.* 58, 151–158.
- Nanou, E., and Catterall, W.A. (2018). Calcium channels, synaptic plasticity, and neuropsychiatric disease. *Neuron* 98, 466–481.
- Nataraj, K., Le Roux, N., Nahmani, M., Lefort, S., and Turrigiano, G. (2010). Visual deprivation suppresses L5 pyramidal neuron excitability by preventing the induction of intrinsic plasticity. *Neuron* 68, 750–762.
- Ringach, D.L., Shapley, R.M., and Hawken, M.J. (2002). Orientation selectivity in macaque V1: diversity and laminar dependence. *J. Neurosci.* 22, 5639–5651.
- Sjöström, P.J., Rancz, E.A., Roth, A., and Häusser, M. (2008). Dendritic excitability and synaptic plasticity. *Physiol. Rev.* 88, 769–840.
- Smith, S.L., Smith, I.T., Branco, T., and Häusser, M. (2013). Dendritic spikes enhance stimulus selectivity in cortical neurons in vivo. *Nature* 503, 115–120.
- Stuart, G.J., and Spruston, N. (2015). Dendritic integration: 60 years of progress. *Nat. Neurosci.* 18, 1713–1721.
- Swindale, N.V. (1998). Orientation tuning curves: empirical description and estimation of parameters. *Biol. Cybern.* 78, 45–56.
- Turrigiano, G.G., and Nelson, S.B. (2004). Homeostatic plasticity in the developing nervous system. *Nat. Rev. Neurosci.* 5, 97–107.
- Turrigiano, G., Abbott, L.F., and Marder, E. (1994). Activity-dependent changes in the intrinsic properties of cultured neurons. *Science* 264, 974–977.
- Wilson, D.E., Whitney, D.E., Scholl, B., and Fitzpatrick, D. (2016). Orientation selectivity and the functional clustering of synaptic inputs in primary visual cortex. *Nat. Neurosci.* 19, 1003–1009.

STAR★METHODS

KEY RESOURCES TABLE

REAGENT or RESOURCE	SOURCE	IDENTIFIER
Deposited Data		
Raw and analyzed data	This paper	https://doi.org/10.17632/hw5p35hc9g.1
Experimental Models: Organisms/Strains		
Mouse: C57BL/6J	National Institute for Medical Research (NIMR), UK	N/A
Software and Algorithms		
MATLAB	https://www.mathworks.com/products/matlab.html	RRID:SCR_001622
FileMaker Pro	https://www.filemaker.com	RRID:SCR_000783
Wavemetrics Igor Pro	https://www.wavemetrics.com/products/igorpro	RRID:SCR_000325
Neuromatic	http://www.neuromatic.thinkrandom.com/	RRID:SCR_004186
Psychophysics Toolbox	http://psycho toolbox.org/	RRID:SCR_002881
IgorR	https://github.com/jefferis/IgorR	N/A

CONTACT FOR REAGENT AND RESOURCE SHARING

Further information and requests for reagents may be directed to and will be fulfilled by the Lead Contact, Troy W. Margrie (t.margrie@ucl.ac.uk).

EXPERIMENTAL MODEL AND SUBJECT DETAILS

All experiments were performed on 5-9 week old black C57BL/6J male mice in accordance with the UK Home Office regulations (Animals [Scientific Procedures] Act 1986) and the Animal Welfare and Ethical Review Body (AWERB).

METHOD DETAILS

Surgical procedures

Mice were anaesthetized with a mixture of fentanyl (0.05mg/kg), midazolam (5.0mg/kg), and medetomidine (0.5mg/kg) in saline solution (0.9%; intraperitoneal). Anaesthesia was checked every 10-15 minutes and supplemented as necessary (20% of initial dose).

During experiments mice were maintained at 37-38°C using a rectal probe and a heating blanket (FHC, Bowdoinham, ME, USA). During surgery both eyes were protected by the application of ointment (Maxitrol, Alcon), which was then carefully removed from the right eye using a cotton bud before visual stimulation (see below). Scalp overlying the left primary visual cortex (V1) was removed and the exposed bone was carefully cleaned and roughened and then allowed to dry fully in the air. A custom-designed head fixation implant was affixed to the skull using a cyanoacrylate-based adhesive (Histoacryl, Braun) and then a dental cement mixture (Simplex Rapid, Kemdent), blackened using 2% carbon powder. During experiments the implant was fixed in a custom-made clamp.

A craniotomy, typically 1x1mm was drilled over V1 using a dental drill (Osada Electric, Japan) with a 0.3mm burr. Following removal of the bone, the exposed dura was carefully washed with cortex buffer until any bleeding had ceased. Bleeding was typically very minor; however, any blood on the surface of the brain dramatically reduced the chance of obtaining a successful gigaseal. In some animals, a small dural incision was performed before recording.

In vivo whole-cell recordings

Patch pipettes for blind *in vivo* whole-cell recordings were fashioned from borosilicate glass (outer diameter: 1.5mm, inner diameter: 0.86mm, Harvard Apparatus) using a two-stage filament puller (PC10, Narashige). The resistance at the tip was 5-7MΩ; any pipettes outside this range were discarded. The tip size of such pipettes was approximately 1.5 μm.

Intracellular solutions for whole-cell recordings was prepared in batches of 2x concentration and frozen in single-use aliquots at -20°C for one month or less, or -80°C for longer periods. The final concentrations (1x) were (all from Sigma-Aldrich or VWR International, UK; in mM) 110 K⁺, 8.5 Na⁺, 5 Mg²⁺, 0.04 Ca²⁺, 110 MeSO₃⁻, 12.04 Cl⁻, 0.05 EGTA, 40 HEPES, 4 ATP, and 0.5 GTP; the pH was adjusted to 7.28 using KOH and/or HCl. On the day of the experiment, the stock was diluted to 1x, and measured for osmolality (mean 289mOsm ± 3.64, range 281-295mOsm) using a vapor osmometer (Vapro 5520, Wecor). Once prepared the solution was kept on ice for the duration of the experiment.

Pipettes were placed in a holder attached to a preamplifier (HS-2A, Axon), mounted on a manipulator (4-axis Junior, Luigs & Neumann) and connected to an Axoclamp 2B amplifier (Axon). Moderate pressure was applied as pipettes were lowered to the brain surface under a 10x water-dipping objective (Olympus), and then rapidly advanced to ~ 200 μm from the pial surface. Positive pressure was then reduced to approximately 30mbar and cell search carried out in voltage-clamp mode (Margrie et al., 2002).

Once whole-cell access was obtained, the amplifier was switched to current-clamp mode and the series resistance was compensated for manually using a bridge circuit. Access resistance was in the range of 15–55M Ω (mean $30.3 \pm 9.4\text{M}\Omega$, $n = 150$). All the experiments described here were carried out in current-clamp mode, with no holding current. Junction potential was not corrected for. Data were low-pass filtered by the amplifier at 10kHz and acquired at 25kHz using an ITC-18 interface (Instrutech) using IGOR Pro software (Wavemetrics) running the Neuromatic package (available at <http://www.neuromatic.thinkrandom.com/>). Electrical (50Hz) noise was minimized by passive electromagnetic shielding of the sample and pre-amplifier. Additionally, a HumBug device (Quest Scientific) was used to further reduce any residual 50Hz electrical noise.

In the control dataset, 110 mice (age range: P34–65) were used and between 1 and 4 neurons were recorded in each mouse (1 neuron: 79 mice; 2 neurons: 24 mice; 3 neurons: 5 mice; 4 neurons: 2 mice) (see below for the visual deprivation group).

Response to current injection

Once stable access to a cell was obtained and the bridge compensation set, an IV protocol was carried out. Square wave current pulses of 1000ms duration were applied, beginning with a hyperpolarising step of -400pA with decrements of 50pA, until the 9th step in which no current was injected. From the 10th step, depolarising current steps with increments of 25 pA were used. Supra-threshold current steps were carried out up to at least 1.5x rheobase.

Visual stimulation

Visual stimulation was carried out using an 8" monitor (ADP-1081AT, DataSound Laboratories) positioned 9cm from the animals left eye, subtending approximately $\pm 42^\circ$ in azimuth and $\pm 34^\circ$ in elevation, positioned at $\sim 45^\circ$ to the long body-axis. A photodiode was positioned over the lower-left corner of the monitor and data were acquired in parallel with electrophysiological recordings to provide an accurate stimulus timestamp. Stimuli were generated using scripts written in MATLAB (Mathworks) using the Psychophysics Toolbox (version 3, <http://psychtoolbox.org/>). Stimuli were generated on a dedicated computer to ensure reliable performance.

Drifting grating stimuli consisted of square wave full-contrast gratings. Grating stimuli consisted of a stationary oriented grating ('hold') for 2 s, followed by a sustained period of drifting grating (2.5 s), followed directly by the next stationary grating. 12 evenly spaced directions were presented with a spatial frequency of 0.0283 cycles per visual degree, and a temporal frequency of 2 cycles per second. Between three and 15 repetitions of the 12 directions were presented.

Visual deprivation

For experiments involving visual deprivation, animals were transferred to cages with fully blackened walls at post-natal day 19 (P19), immediately after weaning (but after eye-opening which occurs at P13–14) and thus includes the critical period (Levelt and Hübener, 2012). This age was chosen in order to introduce a perturbation to the visual network by reducing the visual input for a significant period of time, rather than attempting to ensure that the animal had never experienced any visual stimulation. In total, 13 mice were used in the visual deprivation condition and between 1 and 5 neurons were recorded in each mouse (1 neuron: 3 mice; 2 neurons: 2 mice; 3 neurons: 2 mice; 4 neurons: 3 mice; 5 neurons: 3 mice). The cages were blackened with several layers of matt black emulsion, and covered with a blackout curtain (Thorlabs) to ensure no light could enter around the edges. The blackening of the cages was tested using a light meter (X-Cite XR2100), revealing that minimal light was transmitted through the cage walls even in strong sunlight ($< 0.005 \mu\text{W}/\text{m}^2$). Animals were kept in full darkness until the experiment day, with the exception of brief checks for food and water replenishment which were carried out under low intensity red light.

On the day of the experiment, animals were anaesthetised under red light and placed in a black-out box until the anesthetic had taken full effect. The eyes were then covered with cream then were further covered in with blackout material to avoid exposure to surgical lighting. This material was not removed until immediately prior to the experiment.

Experiments on visually deprived (VD) animals were performed at P37–53 (18–34 days after onset of visual deprivation). As the age profile of the VD animal cohort did not precisely match that of the control dataset, all variables described were tested for correlation with age; none were significantly correlated.

Data Analysis

All experiments were logged in a central database (FileMaker Pro, FileMaker) and were analyzed using MATLAB (Mathworks). Electrophysiological data were imported from Igor PXP format and read in to MATLAB using a custom-written package, based on a similar R package (available at: <https://github.com/jefferis/IgorR>). Action potentials (APs, 'spikes') were detected using a two-step algorithm. First, spikes were detected by finding peaks of dV/dt greater than a threshold of 8x the standard deviation of a 100ms baseline period at the start of the trace. Spike threshold was defined as the membrane potential (V_m) at maximal d^2V/dt^2 up to 4ms before this point. Results of the spike detection procedure were manually verified in all cases. Before any analysis of intrinsic or evoked membrane potential properties, spikes were clipped by removing data points from 1ms before spike threshold till 10ms after and linearly interpolating. All references to V_m values/changes in this text refer to spike-clipped data.

In order to classify regular spiking neurons, we analyzed the waveform of the first evoked AP at rheobase. The only parameters used in classification were the amplitude and time-to-peak of the after-hyperpolarisation (AHP). AHP amplitude was defined as the peak hyperpolarisation within 10ms of the peak of the spike, relative to the steady-state membrane potential ($V_{m_{ss}}$) of the neuron at rheobase. $V_{m_{ss}}$ (the mean V_m between 250 to 50ms before the end of the IV current-step) was used as the baseline measure for calculating AHP amplitude rather than spike threshold, as some neurons displayed a prominent, long-lasting ramp potential before reaching spike threshold, which then artificially increased the estimate of AHP amplitude.

Neurons were classed as regular spiking (RS) if their AHP amplitude was $< 5\text{mV}$, and occurred within 10ms following the peak spike depolarization. All the data in this study were therefore obtained from regular-spiking neurons.

For analysis of intrinsic properties (Figure 1) we performed the following analyses. The resting membrane potential (RMP) was taken as the $V_{m_{ss}}$ of the voltage trace when no current was injected. Rheobase was taken as the first positive current step to elicit a spike. The spike threshold was taken as the threshold of the first spike observed at rheobase. Hyperpolarizing input resistance was calculated at -200pA current injection step. Depolarizing input resistance was calculated at 150pA current injection step and only neurons with a rheobase $> 150\text{pA}$ were included in the calculation (control: $n = 128$, V.D: $n = 35$ cells).

For analysis of visually-evoked responses (Figure 2), the membrane potential response to each direction was divided into a “baseline” window (the final 500ms of the static grating stimulus, before stimulus drift onset) and a “stimulus-evoked” window (0.5-2.5 s after drift onset).

The mean membrane potential response of a neuron to stimulation (V_{m_0}) was defined as follows. For each trial, i , for each direction, θ , $V_{m_0}(i, \theta)$ was calculated as:

$$V_{m_0}(i, \theta) = V_{m_{evoked}}(i, \theta) - V_{m_{baseline}}(i, \theta)$$

where $V_{m_{baseline}}$ is the mean membrane potential during the baseline window, and $V_{m_{evoked}}$ is the mean membrane potential during the stimulus-evoked window.

One concern with this definition is that $V_{m_{baseline}}$ may differ in an orientation selective manner - in other words, that a neuron’s steady-state membrane potential is tuned for stationary grating stimuli. Such an orientation-dependent baseline measure may introduce an apparent tuning in a cell not otherwise tuned for drift orientation, or mask the orientation tuning of a cell which is tuned. To investigate this possibility, the probability of the baseline of each neuron being tuned was calculated using a one-way ANOVA, testing the hypothesis that the baseline differed across orientation conditions. At the 0.05 significance level only 3/128 were found to have a baseline which varied across conditions, fewer than the predicted number of type I errors. Indeed, fewer cells were found to have a stimulus-responsive baseline than would be predicted by the type I error rate at all significance levels. Therefore, it is unlikely the baseline measure used here influences the tuning for orientation as measured to drifting gratings.

The membrane potential modulation of a neuron (V_{m_1}) was quantified as follows. For each direction, the membrane potential responses during the stimulus-evoked window was averaged across trials. Next, the stimulus-evoked window was divided into four separate regions (each 0.5 s long) and the traces in these regions were averaged (giving the average response to a full cycle of the drifting grating). Finally, the membrane potential modulation (V_{m_1}) was taken to be the voltage difference between the maximum and minimum of the averaged trace.

Neurons were classified as responsive to drifting gratings based upon whether changes in mean firing rate during the drifting gratings were statistically significant. First, spiking responses, F_0 , were calculated, for each trial, i , and each direction, θ , as:

$$F_0(i, \theta) = F_{evoked}(i, \theta) - \bar{F}_{baseline}$$

where $\bar{F}_{baseline}$ is the firing rate across all baseline periods (all trials, all directions), and F_{evoked} is the firing rate during the stimulus-evoked window (thus, F_0 can take negative values). Next, for each neuron, a Wilcoxon sign-rank test was performed on the distribution of $|F_0|$ values, to determine whether the stimulus-evoked firing rate was significantly different from baseline.

To calculate the Orientation Selectivity Index (OSI) we used vector methods. First, we computed the normalized vector average of the responses over orientation space (Swindale, 1998; Ringach et al., 2002):

$$OSI = \min\left(\left|\frac{\sum_{\theta} r(\theta) \exp(2i\theta)}{\sum_{\theta} r(\theta)}\right|, 1\right)$$

where $r(\theta)$ are responses to each direction, θ . Three measures of OSI were calculated. OSI_{F_0} was calculated by taking $r(\theta)$ to be the trial-averaged spiking responses (F_0):

$$r(\theta) = \frac{1}{T} \sum_{i=1}^T F_0(i, \theta),$$

$OSI_{V_{m_0}}$ was calculated by taking the trial-averaged mean membrane potential response (V_{m_0}):

$$r(\theta) = \frac{1}{T} \sum_{i=1}^T V_{m_0}(i, \theta),$$

and OSI_{Vm1} by taking $r(\theta)$ to be the membrane potential modulation (Vm_1) as computed above:

$$r(\theta) = Vm_1(\theta).$$

Only cells classified as responsive to drifting gratings (see above) were used to calculate OSI_{F0} (control: $n = 111$, V.D.: $n = 25$). The OSI could exceed 1 (due to negative responses after baseline subtraction) and in such cases we set the value to 1 (control: 3/111 cells, V.D.: 0/25 cells).

In order to consider responses at the preferred direction, preferred direction was calculated in the following way. The preferred orientation was taken as:

$$\text{preferred orientation} = \frac{1}{2} \arg \left(\frac{\sum_{\theta} r(\theta) \exp(2i\theta)}{\sum_{\theta} r(\theta)} \right)$$

Responses were then considered at the grating directions closest to the preferred orientation and to the preferred orientation + 180°. The preferred direction was defined as the grating direction that elicited the largest response. For example, a neuron with a preferred orientation of 20° would have a preferred direction of 210° if the response to drifting gratings at 210° exceeded the response to gratings at 30°; otherwise the preferred direction would be defined as 30°.

QUANTIFICATION AND STATISTICAL ANALYSIS

All statistical analyses were carried out in MATLAB. Statistical details of experiments can be found in the [Results](#) section and in figure legends. The median and interquartile range are reported when comparing the intrinsic and evoked properties of control and visually deprived groups. In order to compare these medians statistically we used the Wilcoxon rank-sum test. For all correlation analyses we used Spearman's rank-order correlation. In order to test for differences in correlation values between control and visually deprived groups we used a direct application of Fisher's Z-transformation. In order to test for differences in the OSI distributions between control and visually deprived groups we used the Kolmogorov-Smirnov test. As we recorded few neurons per animal, neurons were pooled across animals for statistical analyses. We also analyzed the data by animal, using a linear mixed effects model with lighting condition as a fixed effect and subject as a random effect (to account for the fact that repeated-measures from the same animal are not independent). To assess whether there were significant differences between control and visual deprivation condition we compared the model with and without the fixed effect of lighting condition using a Likelihood Ratio Test to generate a p value. This analysis did not change any of the results in the manuscript. Statistical significance level was set at $p = 0.05$ and the exact p value reported, except in figures where p values greater than 0.05 were labeled n.s. (not significant).

DATA AND SOFTWARE AVAILABILITY

The data and code supporting the results are available from Mendeley Data (<https://doi.org/10.17632/hw5p35hc9g.1>).